Polarized deuteron capture by ^{3}He and ^{3}H at and above the fusion resonance region

M. J. Balbes,* J. C. Riley,† G. Feldman,‡ and H. R. Weller
Duke University, Durham, North Carolina 27706
and Triangle Universities Nuclear Laboratory, Durham, North Carolina 27706

D. R. Tilley
North Carolina State University, Raleigh, North Carolina 27695
and Triangle Universities Nuclear Laboratory, Durham, North Carolina 27706
(Received 16 March 1993)

The absolute differential cross sections and vector and tensor analyzing powers for the ^{3}He$(\vec{d},\gamma)^5$Li and ^{3}H$(\vec{d},\gamma)^5$He reactions have been measured both in the $j^\pi = \frac{3}{2}^+$ fusion resonance region [E_d(lab)=0.45 MeV and E_d(lab)=0.1 MeV, respectively] and at E_d(lab)=8.6 MeV for several angles. In the fusion resonance region, a transition matrix element (TME) analysis of the observables leads to multiple solutions for both reactions, all of which indicate that the reactions proceed predominantly through s-wave ($E1$) capture, with small admixtures of $M1$ or $E2$ radiation. One solution for each reaction is dominated by a large (~90%) $^4s_{3/2}(E1)$ capture strength. Coupled-channels resonating group model (CCRGM) calculations have been performed which favor these solutions. In the CCRGM picture, the $j^\pi = \frac{3}{2}^+$ fusion resonance in the capture cross section is a consequence of the tensor force, which couples the $s = \frac{3}{2}$, d+^{3}He (or d+^{3}H) channel to the $s = \frac{1}{2}$, p+^{4}He (or n+^{4}He) channel, enabling the reactions to proceed via the spin-independent ($E1$) transition to the ground state. At E_d(lab)=8.6 MeV, a TME analysis of the ^{3}He$(\vec{d},\gamma)^5$Li reaction yields a single solution which has >80% s-wave ($E1$) capture strength, whereas two TME solutions exist for the ^{3}H$(\vec{d},\gamma)^5$He reaction with 45% and 65% s-wave ($E1$) capture strength. These data are also compared to the results of the CCRGM calculations.

PACS number(s): 21.45.+v, 23.20.En, 23.20.Js, 25.40.Lw

I. INTRODUCTION

The d+^{3}He and d+^{3}H reactions have been studied in considerable detail because of their potential for being used as a fuel in an energy-producing fusion reactor. In both reactions, the energy yield is enhanced by the $j^\pi = \frac{3}{2}^+$ resonance (called the fusion resonance) which exists just above fusion reactor energies. Although the d+^{3}He reaction offers a cleaner source of energy since only stable elements are involved in the reaction and no neutrons are produced, current fusion technology relies on the d+^{3}H reaction due to the lower ignition temperature. In the d+^{3}H reactors which are being designed and studied today, the ^{3}He$(d,\gamma)^5$Li reaction is being considered as a possible diagnostic for the plasma. The reaction comes about from the deuterium fusing with ^{3}He, which is created in the $d(d,n)^3$He reaction. The γ-ray yield from this reaction, along with the previously measured ^{3}He$(d,\gamma)^5$Li-to-^{3}He$(d,p)^4$He branching ratio, gives a direct measure of the fusion energy production rate of the reactor [1].

The properties of the fusion resonances in ^{5}Li and ^{5}He have been determined by studies of the ^{3}He$(d,p)^4$He and ^{3}H$(d,n)^4$He reactions [2–7]. The isotropic angular distributions of the cross sections indicate that the resonances are formed via s-wave capture and therefore have positive parity. Since the spin of the deuteron ($S = 1$) can couple with the spins of ^{3}He or ^{3}H ($S = \frac{1}{2}$) to form channel spins of $s = \frac{1}{2}$ or $\frac{3}{2}$, the total angular momentum ($j = 1 + s$) of the fusion resonance can only be $j^\pi = \frac{1}{2}^+$ or $j^\pi = \frac{3}{2}^+$. Phase shift analyses of the ^{4}He$(p,p)^4$He reaction [8–10] have confirmed the original spin and parity assignment of $j^\pi = \frac{3}{2}^+$ which was obtained from the unitarity condition. (We have adopted the convention that uppercase letters refer to the ground state and lowercase letters refer to the scattering state.)

Shell-model calculations predict a $\frac{3}{2}^+$ state (the fusion resonance) above a $\frac{1}{2}^+$ state at excitation energies above the $\frac{1}{2}^-$ first excited state [11]. Coupled-channels calculations disperse the strength of the $\frac{1}{2}^+$ state because it couples strongly to the $\alpha + N$ channel (where $N = p$ or n) [12,13]. The $\frac{3}{2}^+$ state, however, couples to the $\alpha + N$ channel only through the tensor and spin-orbit forces and therefore has a relatively narrow width [14]. Coupled-channels resonating group model calculations in the fusion resonance region also require the presence of a

*Current address: Dept. of Physics, Ohio State University, 174 W. 18th Ave., Columbus, OH 43210.
†Current address: Dept. of Physics, University of South Carolina–Spartanburg, 800 University Way, Spartanburg, SC 29303.
‡Current address: Saskatchewan Accelerator Laboratory, University of Saskatchewan, Saskatoon, Canada S7N 0W0.

tensor force to predict the strength of the ^{3}He$(d,p)^4$He and ^{3}H$(d,n)^4$He low-energy cross sections [15].

Capture reactions with polarized deuterons are well suited for probing tensor-force effects in the $j^\pi = \frac{3}{2}^+$ fusion resonance regions of ^{5}Li and ^{5}He because of the constraints imposed by the spin-independence selection rule for $E1$ radiation, which says that the dominant term of the $E1$ operator does not affect intrinsic spin. As stated above, this resonance is populated predominantly by s-wave deuterons in the $s = \frac{3}{2}$ channel. The $J^\pi = \frac{3}{2}^-$ ground states of ^{5}Li and ^{5}He, on the other hand, are predominantly $^2P_{3/2}$ states (using the notation $^{2S+1}L_J$) as seen in the L-S coupled single-particle model where the ground states consist predominantly of a nucleon in the $L = 1$ orbital above a closed 0^+ ^{4}He core. Therefore, in keeping with the spin-independence selection rule, there are at least two likely mechanisms for an $E1$ γ-ray transition from the predominantly $s = \frac{3}{2}$ resonance to the predominantly $S = \frac{1}{2}$ ground state: (1) the $s = \frac{3}{2}$ resonance can decay directly to the $S = \frac{3}{2}$ component of the ground state which may be present due to tensor-force mixing in the ground state, or (2) the tensor force can mix the $s = \frac{3}{2}$ and $\frac{1}{2}$ scattering states with the same j^π, allowing the transition to the $S = \frac{1}{2}$ component of the ground state.

The cross section for the ^{3}He$(d,\gamma)^5$Li reaction was first measured by Blair, Hintz, and Van Patter [16]. An excitation-function measurement showed the fusion resonance at E_d(lab)=0.45 MeV with an angle-integrated total cross section of 50 ± 10 μb. An angular distribution taken at E_d=0.58 MeV was consistent with isotropy to within 10%. Buss *et al.* [17] also measured an isotropic angular distribution (at E_d=0.48 MeV) but claim a lower total cross section of 21 ± 4 μb. Krauss, Suffert, and Magnac-Valette [18] measured an excitation function at 90° and, assuming an isotropic angular distribution, obtained a total cross section of 38 μb at resonance. Cross sections and branching ratios of the ^{3}H$(d,\gamma)^5$He reaction measured below 1 MeV [19–23] find that the d+^{3}H fusion resonance lies at E_d(lab)=107 keV. Buss, Waffler, and Ziegler [19] derived a total on-resonance cross section of 60 μb.

Above the fusion resonance, the ^{3}He$(d,\gamma)^5$Li reaction in the range E_d=2–26 MeV has been the basis of many studies [24–28]. Tombrello, Spiger, and Bacher [24] suggest the existence of a broad state at 20 MeV with a possible spin assignment of $\frac{3}{2}^+$ or $\frac{5}{2}^+$, whereas Schröder and Mausberg [25] also consider a spin assignment of $\frac{1}{2}^+$. Del Bianco *et al.* [26] found no clear evidence for the existence of any state at this energy. King [27] measured an excitation function from 17 MeV$\leq E^*_{^5\mathrm{Li}} \leq$ 26 MeV as well as several angular distributions within this energy range. The analysis of the γ_0 and γ_1 transition strengths was consistent with a $\frac{1}{2}^+$ state around 18 MeV and a $\frac{5}{2}^+$ state around 20 MeV. Similar levels have been seen in ^{5}He [28]. If such states do exist, then the current experiments at E_d(lab)=8.6 MeV ($E^*_{^5\mathrm{Li}}$ = 21.5 MeV and $E^*_{^5\mathrm{He}}$ = 21.9 MeV) lie on the high-energy sides of these 20 MeV resonances.

The analyzing powers of the ^{3}He$(\vec{d},\gamma)^5$Li and the ^{3}H$(\vec{d},\gamma)^5$He reactions have not been measured previously, although brief summaries of our current experiments have already been published [29,30]. This paper presents the results of our recently concluded study of these reactions. Cross sections and vector and tensor analyzing powers of the ^{3}He$(\vec{d},\gamma)^5$Li reaction have been measured with a deuteron beam at E_d(lab)=0.8 MeV, which was stopped in the target (thus integrating over most of the fusion resonance), at E_d(lab)=0.6 MeV, which lost 0.3 MeV in the target (therefore spanning the full width at half maximum of the fusion resonance), and at E_d(lab)=8.6 MeV. Cross sections and analyzing powers of the ^{3}H$(\vec{d},\gamma)^5$He reaction have been measured with a deuteron beam at E_d(lab)=0.4 MeV, which was stopped in the target, and at E_d(lab)=8.6 MeV. The results of Legendre polynomial and transition matrix element fits to the data are presented as well as coupled-channels resonating group model calculations which were performed in both energy regions. Finally, conclusions about the reactions and the role of the tensor force will be discussed.

II. EXPERIMENTAL TECHNIQUES

In the present work, polarized beams were produced at the Triangle Universities Nuclear Laboratory (TUNL) using both the Lamb-Shift Polarized Ion Source [31] and, in the later stages, the new Intense Polarized Ion Source [32]. The beam polarization obtained from each source was measured using, respectively, the quench-ratio method [5] and a polarimeter utilizing the ^{3}He$(d,p)^4$He reaction [33]. Capture γ rays were detected in two 25.4 cm×25.4 cm NaI(Tl) spectrometers [34] with active and passive shielding, and with known efficiencies and lineshape response functions [30].

For the ^{3}He$(\vec{d},\gamma)^5$Li reaction study above the fusion resonance region, an 8.85 MeV beam from the accelerator was used to create 8.6 MeV deuterons at the center of the target. This beam was pulsed at 5 MHz in order to allow time-of-flight discrimination between neutron and γ-ray events in the NaI spectrometer. The gaseous ^{3}He target [35] was operated at a pressure of 69.0 kPa with a 1.27 μm Nickel beam-entrance foil and a 2.54 μm Havar beam-exit foil. Lead and tungsten shadow bars were used to prevent the NaI spectrometers from directly viewing these foils and allowed the spectrometers to see a region of gas which was 3.58 cm long when the spectrometer was at 90°, corresponding to a target thickness of 0.301 mg/cm^2 and a solid angle of 23 msr. As an additional monitor of the experiment, an Ortec transmission-mount 500-μm-thick solid-state detector was placed in the target chamber at 30° and was doubly collimated to view the center of the target. For the ^{3}H$(\vec{d},\gamma)^5$He experiment, the beam was pulsed at 4 MHz and was passed through a tritiated titanium target which contained approximately 240 μg/cm^2 of tritium. Again, shadow bars were used to reduce background, but it was not possible to mount a monitor detector inside the target chamber due to geometrical constraints.

For the experiments in the fusion resonance regions, it was necessary to degrade the beam energy using Havar foils since the accelerator cannot produce beams below ~ 2 MeV. In order to set the beam energy, the deuteron beam was scattered from a thin (~ 10 $\mu g/cm^2$) ^{12}C foil into a calibrated solid-state detector located at $\theta_{ss} = 30°$. The procedure for creating a 0.8 MeV beam began by rotating four Havar degrading foils (6.35 μm thick) into position between the target and the detector. The accelerator voltage was then adjusted to give a 0.8 MeV deuteron peak in the solid-state detector spectrum. The foils were rotated out of position, giving an undegraded scattered-deuteron peak with an energy of 3.43 MeV. Figure 1 shows the spectra for the undegraded and degraded scattered-deuteron peak. To obtain these same conditions for the capture experiments, the beam energy was adjusted such that a 3.275 MeV scattered-deuteron peak was seen in the solid-state detector spectrum, indicating that the incident beam energy was 3.43 MeV. Finally, these same Havar degrading foils were transferred back to the capture setup to ensure uniformity in foil thickness. The above procedure was also used to produce deuteron beams with energies of 0.8 ± 0.09, 0.6 ± 0.08, and 0.4 ± 0.1 MeV, where the uncertainties are given by half of the FWHM of the peaks seen in the solid-state detector spectra. The uncertainty in the centroid energy is estimated to be ± 0.02 MeV, based on the uncertainty in the calibration of the solid-state detector.

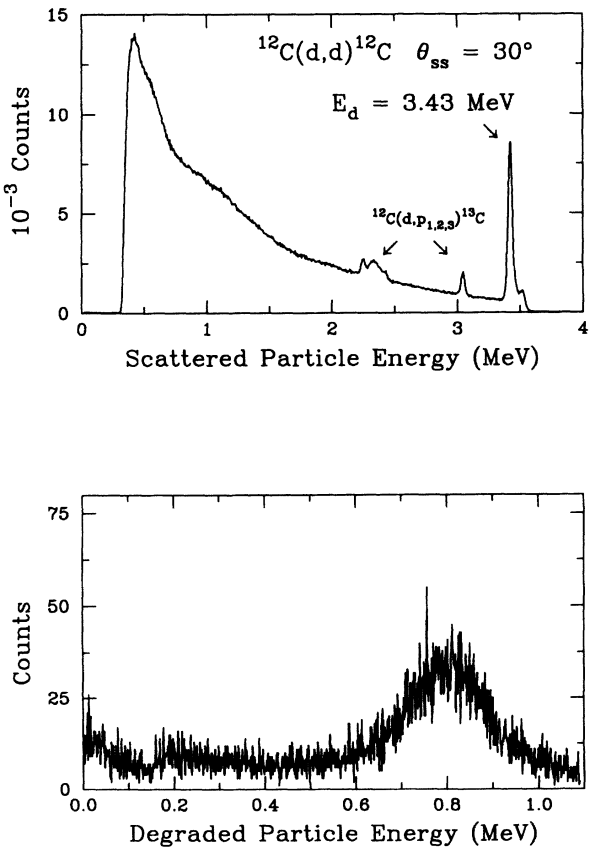

FIG. 1. Upper panel: Solid-state detector spectrum from the $^{12}C(d,d)^{12}C$ reaction. Lower panel: Spectrum from the above reaction where Havar degrading foils have been placed in front of the detector. The resultant deuterons have an energy of 0.8 MeV.

In order to determine the gas pressures needed for the ^{3}He target for measurements in the fusion resonance region, the solid-state detector was placed inside a small vacuum chamber with a Havar entrance foil and the whole assembly was placed inside the scattering chamber. The scattered-deuteron energy was set by evacuating the chamber and adjusting the accelerator voltage such that the deuterons incident on the solid-state detector had the proper energy. The chamber was then pressurized in small increments with ^{3}He until the deuterons reaching the detector had lost the desired energy in the gas. Using this procedure, it was determined that 414 kPa of ^{3}He gas would completely stop the 0.8 MeV deuteron beam in the target and that 156 kPa of gas would degrade the 0.6 MeV beam to an energy of 0.30 ± 0.14 MeV, where the uncertainty represents half of the FWHM of the deuteron peak as seen in the solid-state detector spectrum. As before, the centroid uncertainty is estimated to be ± 0.02 MeV.

The ^{3}He target for the experiments in the fusion resonance region consisted of a 2.54 cm long cylindrical gas cell [36] with the degrading foils described above mounted as the entrance window. The cell was filled with either 414 or 156 kPa of research grade 99.95% pure ^{3}He gas. These gas pressures correspond to target thicknesses of $(1.54 \pm 0.14) \times 10^{20}$ atoms/cm^2 and $(5.82 \pm 0.15) \times 10^{19}$ atoms/cm^2, respectively. The errors in the target thicknesses were calculated from the uncertainties in the target length, gas pressure, and gas temperature. Note that the target length uncertainty is much smaller when the beam is stopped in the back wall of the target cell than when it is stopped in the gas. Accurate beam-current integration was achieved by electrically isolating the gas cell and applying a suppression voltage to prevent the escape of secondary electrons. Background spectra were obtained by replacing the ^{3}He with an equal pressure of ^{4}He to maintain the energy loss of the deuterons through the gas. Although beam depolarization in the gaseous ^{3}He target was a concern, previous measurements have shown that this is not a large effect [36].

For the $^3H(\vec{d},\gamma)^5He$ experiment, a 3.375 MeV deuteron beam was passed through a 25.4 μm Havar foil to degrade the beam energy to 0.4 MeV with an energy spread of 0.2 MeV FWHM. The beam was pulsed at 4 MHz to create a time-of-flight condition which was used to reduce the neutron background. The beam was then stopped in a tritiated titanium foil which contained approximately 1 mg/cm^2 of tritium. Background spectra were measured using a pure titanium target of comparable thickness and, after normalizing them using the $Ti(p,p)Ti$ yields from the solid-state spectra, they were subtracted from the spectra obtained with the tritiated foil.

In order to measure the cross sections and analyzing powers of both capture reactions with the TUNL Lamb-Shift Polarized Ion Source, the beam was polarized along the quantization axis ζ (longitudinal out of the source) into State 1, 2, or 3 where the polarization [5] in State 1 is $p_\zeta = Q$ and $p_{\zeta\zeta} = Q$; for State 2, $p_\zeta = 0$ and $p_{\zeta\zeta} = -2Q$;

for State 3, $p_\zeta = -Q$ and $p_{\zeta\zeta} = Q$. Q represents the fraction of the beam which is polarized as measured with the quench-ratio method. When the quantization axis is rotated perpendicular to the reaction plane by a Wien filter, the cross section and analyzing powers are given by

$$\sigma_0(\theta) = \tfrac{1}{3}[\sigma_1(\theta) + \sigma_2(\theta) + \sigma_3(\theta)], \tag{1}$$

$$A_y(\theta) = \frac{1}{Q}\left(\frac{\sigma_1(\theta) - \sigma_3(\theta)}{\sigma_1(\theta) + \sigma_2(\theta) + \sigma_3(\theta)}\right), \tag{2}$$

$$A_{yy}(\theta) = \frac{1}{Q}\left(\frac{\sigma_1(\theta) + \sigma_3(\theta) - 2\sigma_2(\theta)}{\sigma_1(\theta) + \sigma_2(\theta) + \sigma_3(\theta)}\right), \tag{3}$$

where

$$\sigma_i(\theta) = \sigma_0(\theta)[1 + \tfrac{3}{2}p_\zeta(i)A_y(\theta) + \tfrac{1}{2}p_{\zeta\zeta}(i)A_{yy}(\theta)]$$

denotes the polarized cross section in state i ($i = 1, 2, 3$). The ^{3}He$(\vec{d},\gamma)^5$Li observables $\sigma(\theta)$, $A_y(\theta)$, and $A_{yy}(\theta)$ at 8.6 and 0.8 MeV were determined, as were the ^{3}H$(\vec{d},\gamma)^5$He observables at 0.4 MeV, by making sequential measurements in States 1, 2, and 3, and then solving the above equations. Each measurement typically lasted from 1 to 2 hours with eight runs total at each angle, two each for States 1 and 3, and four runs in State 2 in order to optimize the statistical error.

A pure vector-polarized beam from the Lamb-Shift source with the quantization axis oriented perpendicular to the reaction plane was used to measure $A_y(\theta)$ for the ^{3}H$(\vec{d},\gamma)^5$He reaction at E_d(lab)=8.6 MeV. In this mode $A_y(\theta)$ is given by

$$A_y(\theta) = \frac{1}{Q}\frac{\sigma^+(\theta) - \sigma^-(\theta)}{\sigma^+(\theta) + \sigma^-(\theta)}, \tag{4}$$

where $\sigma^+(\theta)$ and $\sigma^-(\theta)$ denote cross sections measured with spin up and spin down, respectively. Similarly, a pure tensor-polarized beam was used to measure $T_{20}(\theta)$ for this reaction at 8.6 MeV according to the expression

$$T_{20}(\theta) = \frac{\sqrt{2}}{Q}\frac{\sigma_1(\theta) - \sigma_0(\theta)}{2\sigma_1(\theta) + \sigma_0(\theta)}, \tag{5}$$

where σ_0 denotes the unpolarized cross section and σ_1 is defined above.

To measure $A_y(\theta)$ and $A_{yy}(\theta)$ at 0.6 MeV, and $T_{20}(\theta)$ at 0.8 MeV for the ^{3}He$(\vec{d},\gamma)^5$Li reaction using the Intense Polarized Ion Source, the beam was polarized using the Strong Field 2, $3 \leftrightarrow 5$ transition [32]. The theoretical maxima for the beam moments are $p_\zeta = \frac{1}{3}$ and $p_{\zeta\zeta} = -1$, respectively. Typically, the actual polarizations are about 80% of these values. Since the polarization of the beam out of this source was measured with a polarimeter [33], it is natural to describe it in terms of the polarization moments p_ζ and $p_{\zeta\zeta}$ [5], where the quantization axis ζ is perpendicular to the reaction plane in the case of measuring $A_y(\theta)$ and $A_{yy}(\theta)$, and parallel to the beam momentum when measuring $T_{20}(\theta)$. The analyzing powers were obtained by measuring the polarized cross section $\sigma_P(\theta)$ using the above polarization moments and the unpolarized cross section $\sigma_0(\theta)$ for a left and right detector. The expressions for the analyzing powers then become

$$A_y(\theta) = \frac{1}{3p_\zeta}\left(\frac{\sigma_{LP}(\theta)}{\sigma_{L0}(\theta)} - \frac{\sigma_{RP}(\theta)}{\sigma_{R0}(\theta)}\right), \tag{6}$$

$$A_{yy}(\theta) = \frac{1}{p_{\zeta\zeta}}\left(\frac{\sigma_{LP}(\theta)}{\sigma_{L0}(\theta)} + \frac{\sigma_{RP}(\theta)}{\sigma_{R0}(\theta)} - 2\right), \tag{7}$$

$$T_{20}(\theta) = \frac{\sqrt{2}}{p_{\zeta\zeta}}\left(\frac{\sigma_P(\theta)}{\sigma_0(\theta)} - 1\right), \tag{8}$$

where the L and R subscripts refer to the left and right detectors, respectively. In the case of $T_{20}(\theta)$, they are equivalent.

III. THE FUSION RESONANCE REGION

A. General discussion and formalism

We shall first give an overview of the general techniques of analysis common to both reactions under study, followed by specific discussions for each. Our analyses began with fits of Legendre and associated Legendre polynomials to the observables as defined in Ref. [37]. According to this formalism, the highest-order Legendre polynomial in the series is given by twice the maximum multipolarity of the γ rays. Odd terms in the series are indicative of interference between different multipoles of opposite parity. Further information can be extracted from these data by performing a transition matrix element (TME) analysis. The formalism of Seyler and Weller [37] is used to express the reaction observables in terms of the reduced transition matrix elements (TME's), where the TME's are labeled by their continuum state quantum numbers ($^{2s+1}\ell_j$ in ℓ-s coupling) and the multipolarity ($E\lambda$ or $M\lambda$) of the outgoing γ rays. The relevant TME's are then fit simultaneously to all of the observables at a given energy, giving a model-independent interpretation of the reaction.

In the fusion resonance region, s-wave capture is expected to dominate the reaction due to suppression of higher partial waves by the angular momentum barrier. By considering s-wave capture only, the expressions for the observables in terms of the TME's become:

$$\sigma(\theta) = 2|^2s_{1/2}(E1)|^2 + 4|^4s_{3/2}(E1)|^2, \tag{9}$$

$$A_y(\theta) = 0, \tag{10}$$

and

$$A_{yy}(\theta) = \frac{0.632|^2s_{1/2}(E1)||^4s_{3/2}(E1)|\cos(\delta) + 0.800|^4s_{3/2}(E1)|^2}{2|^2s_{1/2}(E1)|^2 + 4|^4s_{3/2}(E1)|^2}, \quad (11)$$

where δ is the relative phase between the two transition matrix elements. In the $\frac{3}{2}^+$ fusion resonance region, it is expected that the $^4s_{3/2}(E1)$ transition matrix element will dominate the reaction. If the reaction proceeds by pure $^4s_{3/2}(E1)$ capture then $A_{yy}(\theta)$=0.2, whereas if it proceeds by pure $^2s_{1/2}(E1)$ capture then $A_{yy}(\theta)$=0.0. Thus measuring $A_{yy}(\theta)$ provides sensitivity to the admixture of the two transition matrix elements.

In practice, it is necessary to include p-wave terms (either $M1$ or $E2$) in the above expressions in order to fit any fore-aft asymmetry which is present in the data. Unfortunately, an unconstrained inclusion of p-wave capture introduces too many free parameters into the fitting process. In order to maintain a reasonable number of free parameters, the j dependence of the p-wave transition matrix elements has been suppressed in our analysis.

B. The ^{3}He$(\vec{d},\gamma)^5$Li reaction

Observables were measured in two energy ranges about the fusion resonance of ^{5}Li. The absolute cross section $\sigma(\theta)$, the vector analyzing power $A_y(\theta)$, and the tensor analyzing powers $A_{yy}(\theta)$ and $T_{20}(\theta)$ were measured for a deuteron beam at E_d(lab)=0.8 MeV, which was stopped in the target (thus integrating over the entire fusion resonance). The same quantities excluding $T_{20}(\theta)$ were measured for a deuteron beam at E_d(lab)=0.6 MeV which lost 0.3 MeV in the target (integrating over the FWHM of the fusion resonance). Typical spectra including a convolution fit [30,38] and typical summing region are shown in Fig. 2 along with background spectra where ^{4}He was substituted for ^{3}He in the target chamber. The measured observables are plotted in Fig. 3.

The observables in both energy ranges were fit with Legendre and associated Legendre polynomials. Unfortunately, it is not possible to extract the $\bar{c}_k$ and $\bar{e}_k$ coefficients from $A_{yy}(\theta)$ without a measurement of $T_{20}(\theta)$ also, due to the nonorthogonality of the Legendre and second associated Legendre polynomials. Therefore, for the E_d(lab)=0.6 MeV measurement, $A_{yy}(\theta)$ was fit with ordinary Legendre polynomials. The results are presented in Table I. The finite odd coefficients indicate $E1$-$M1$ and/or $E1$-$E2$ interference. The small k=3 and 4 coefficients suggest that the contributions from $E2$ radiation are small. In fact, Legendre polynomials with $k > 2$ are not statistically justified in fits to any of the observables except $\sigma(\theta)T_{22}(\theta)$, where

$$T_{22}(\theta) = -\frac{1}{\sqrt{3}}A_{yy}(\theta) - \frac{1}{\sqrt{6}}T_{20}(\theta),$$

since either χ^2_ν (χ^2 per degree of freedom ν) is not significantly improved or is already less than unity for the fits with $k \leq 2$. Previous angular distribution measurements [16,17] of the cross section in the fusion resonance region have indicated that the cross section is isotropic to within 10%. The cross-section measurements of the present experiment have been determined to be consistent with isotropy to within 5% in a Legendre fit to A_0 only.

The results of a simultaneous TME fit to the observables measured with E_d(lab)=0.8 MeV are given in Tables I and II and shown in Fig. 3. These fits included the $^2s_{1/2}(E1)$ and $^4s_{3/2}(E1)$ terms as well as the $^2p(M1)$ and $^4p(M1)$ terms (where the j dependence of the p-wave terms has been suppressed). Two statistically significant solutions with identical $\chi^2_\nu = 1.25$ have been found, one with dominant $s = \frac{3}{2}$ s-wave capture strength, the second with nearly equal strengths for the $s = \frac{1}{2}$ and $\frac{3}{2}$ s-wave transition matrix elements. Unfortunately, from the analysis alone, it is impossible to choose one solution over the other.

In order to understand the physics of the ^{3}He$(\vec{d},\gamma)^5$Li reaction in the fusion resonance region more fully, angular distributions of $\sigma(\theta)$, $A_y(\theta)$, and $A_{yy}(\theta)$ were measured for a beam energy spread which integrated only over the FWHM of this resonance (from 0.6 to 0.3 MeV in the lab frame). A transition matrix element analysis which uses the same choices of TME's as the fit to

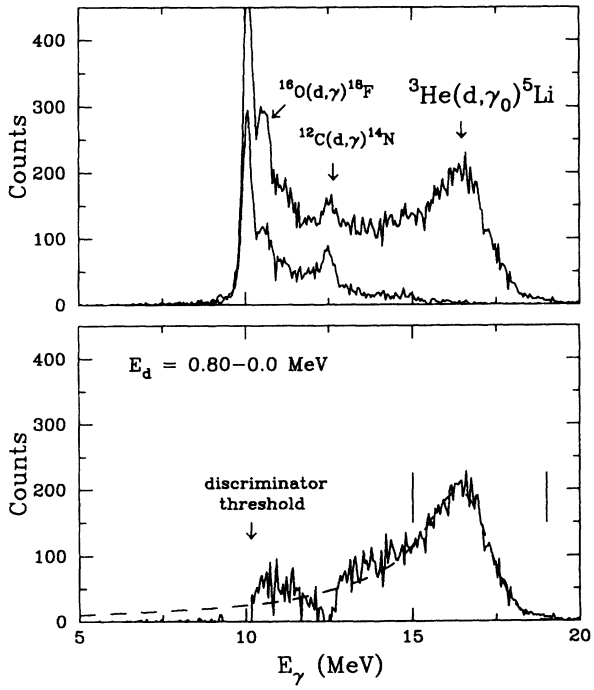

FIG. 2. Upper panel: A γ-ray spectrum from the ^{3}He$(\vec{d},\gamma)^5$Li reaction at E_d(lab)=0.8 MeV. Also shown is a background spectrum which is obtained by replacing the ^{3}He gas target with ^{4}He. Lower panel: The resultant background-subtracted spectrum. The dashed line is the result of a line-shape fit to the data. Vertical lines denote a typical summing region.

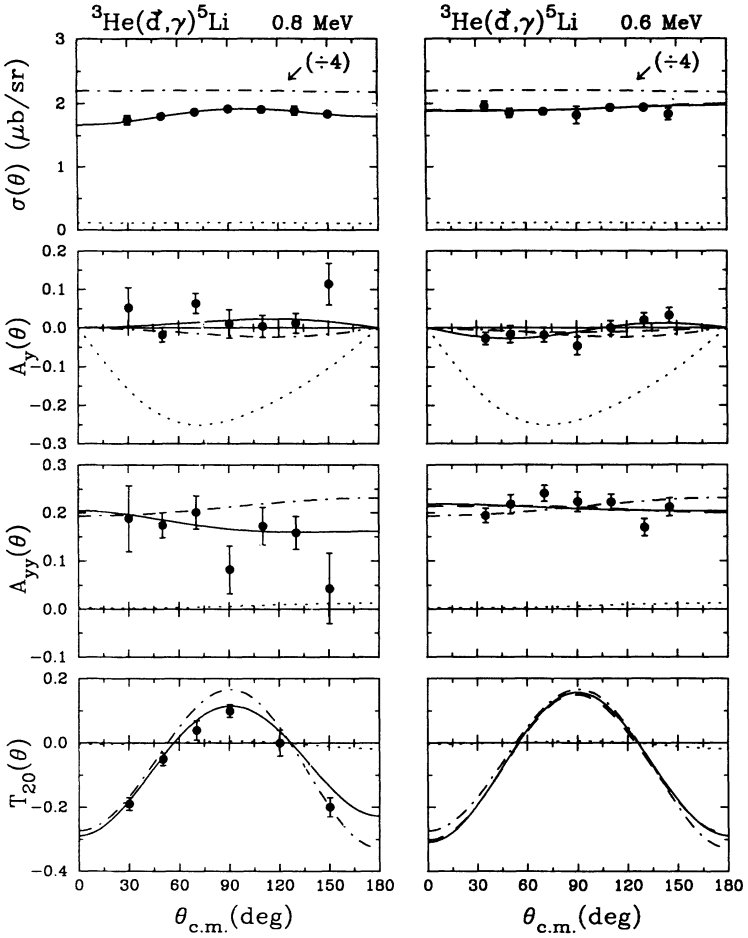

FIG. 3. Left side: Observables measured for the ^{3}He($\vec{d},\gamma$)^{5}Li reaction at E_d(lab)=0.8 MeV where the beam was stopped in the target. The solid curves are the result of two independent transition matrix element fits to the data (see Table II). The two solutions result in curves which are indistinguishable in the figure. The dashed-dotted and dotted curves are from CCRGM calculations A (with the two-body tensor force) and D (no tensor force). Note that the actual CCRGM cross sections are a factor of 4 higher than what is plotted. Right side: The same reaction at E_d(lab)=0.6 MeV where the beam lost 0.3 MeV in the target. The solid curve is from the TME Solution 1 in Table II, and the dashed curve is from solutions 2 and 3 which give identical results (see Table II). The dashed-dotted and dotted curves are from CCRGM calculations A (with the two-body tensor force) and D (no tensor force). Note that the actual CCRGM cross sections are a factor of 4 higher than what is plotted.

TABLE I. Legendre polynomial coefficients for the ^{3}He($\vec{d},\gamma$)^{5}Li reaction at E_d=0.8 MeV and at E_d=0.6 MeV and the ^{3}H($\vec{d},\gamma$)^{5}He reaction at E_d=0.4 MeV in the fusion resonance region from a TME fit to the data, and from the CCRGM calculations. Calculation A uses the two-body potential. Calculation B uses the phase-shift fitted potential. Calculation C uses the two-body potential with the tensor-force strength set to 0.75 times its two-body value. Calculation D uses the two-body potential with no tensor force. A_0 is given in units of μb/sr. Coefficients from a direct fit of Legendre polynomials to the data are given in the footnote when they differ by more than one standard deviation from the TME-fit results.

	^{3}He($\vec{d},\gamma$)^{5}Li						^{3}H($\vec{d},\gamma$)^{5}He			
	E_d=0.8 MeV TME fit	E_d=0.6 MeV TME fit (Solution 2)	RGM A	RGM B	RGM C	RGM D	E_d=0.4 MeV TME fit	RGM A	RGM C	RGM D
A_0	1.85 ±0.13	1.91 ±0.16	8.78	44.95	4.46	0.114		126	59.3	0.528
$\bar{a}_1$	−0.035 ±0.011	−0.025 ±0.221	0.004	0.002	0.006	0.010	−0.002±0.001	0.000	0.001	−0.265
$\bar{a}_2$	−0.065 ±0.017	0.001 ±0.007	−0.005	−0.006	−0.006	−0.050	−0.010±0.020	−0.003	−0.002	−0.008
$\bar{b}_1$	0.031 ±0.020	−0.018 ±0.099	−0.030	−0.007	−0.047	−0.371	0.020±0.038	0.001	0.001	0.019
$\bar{b}_2$	−0.010 ±0.003	0.000 ±0.002	0.007	0.007	0.007	−0.034	0.008±0.003[a]	0.003	0.003	−0.026
$\bar{c}_0$	−0.001 ±0.001[b]	0.000 ±0.001	0.012	0.013	0.012	0.001	−0.004±0.002	0.010	0.010	0.000
$\bar{c}_1$	−0.020 ±0.006	−0.001 ±0.011	0.012	0.002	0.017	0.003	−0.087±0.025	−0.003	−0.005	0.002
$\bar{c}_2$	−0.242 ±0.025	−0.300 ±0.113	−0.310	−0.293	−0.321	−0.011	−0.193±0.023	−0.295	−0.302	−0.011
$\bar{e}_2$	−0.099 ±0.010[b]	−0.122 ±0.046	−0.127	−0.120	−0.131	−0.004	−0.080±0.010	−0.121	−0.123	−0.004

[a] $\bar{b}_2 = -0.005 \pm 0.008$.
[b] $\bar{c}_0 = -0.030 \pm 0.012$, $\bar{e}_2 = -0.046 \pm 0.006$.

TABLE II. Relative contributions of transition matrix elements to the cross section from a TME fit to the cross section and analyzing powers of the ^{3}He$(\vec{d},\gamma)^5$Li reaction in the fusion resonance region. The phase of the $^4s_{3/2}(E1)$ matrix element has been arbitrarily set to zero.

	^{3}He$(\vec{d},\gamma)^5$Li at E_d(lab)=0.8–0.0 MeV TME fits					
	Solution 1 χ^2_ν=1.3		Solution 2 χ^2_ν=1.3		Solution 3 χ^2=1.8	
TME	Intensity	Phase	Intensity	Phase	Intensity	Phase
$^2s_{1/2}(E1)$	0.03±0.03	260°±3°	0.48±0.06	145°±3°		
$^4s_{3/2}(E1)$	0.89±0.03	0°	0.44±0.05	0°		
$^2p(M1)$	0.01±0.01	69°±2°	0.01±0.01	66°±4°		
$^4p(M1)$	0.07±0.02	173°±2°	0.07±0.02	−10°±2°		
	^{3}He$(\vec{d},\gamma)^5$Li at E_d(lab)=0.6–0.3 MeV TME fits					
$^2s_{1/2}(E1)$	0.19±0.17	175°±6°	0.01±0.07	174°±180°	0.45±0.07	8°±20°
$^4s_{3/2}(E1)$	0.67±0.15	0°	0.99±0.08	0°	0.52±0.05	0°
$^2p(M1)$	0.10±0.03	89°±5°				
$^4p(M1)$	0.04±0.02	−24°±9°				
$^2p(E2)$			0.00±0.01	68°±62°	0.02±0.04	−84°±95°
$^4p(E2)$			0.00±0.01	67°±117°	0.01±0.01	−85°±132°

the $E_d = 0.8$ MeV data finds, rather than the two previous solutions, one unique solution with a χ^2_ν=1.4 whose errors nearly span both previous solutions (see Table II). If $E2$ radiation (instead of $M1$) is introduced into the fits to account for the asymmetry of the data, then the set of two solutions is recovered. These fits do not have quite as good a χ^2_ν (=1.8) although they are acceptable from a statistical point of view. The results of these fits are given in Tables I and II and plotted in Fig. 3.

A consistent picture of this reaction in the fusion resonance region is provided by the TME solutions which feature a dominant $^4s_{3/2}(E1)$ matrix element. In integrating just over the peak of the resonance, the reaction proceeds almost completely via the $^4s_{3/2}(E1)$ transition. However, when a larger energy region is sampled, contributions from other transitions (either $M1$ or $E2$) become non-negligible.

C. The ^{3}H$(\vec{d},\gamma)^5$He reaction

The background-subtracted spectra obtained from this reaction were fit with the line-shape response function of the NaI detector. A convolution with a Breit-Wigner function to account for the resonant ground state was not necessary to obtain adequate fits in this case. The relative cross section $\sigma(\theta)/A_0$, the vector analyzing power $A_y(\theta)$, and the tensor analyzing power $A_{yy}(\theta)$ were measured and are plotted in Fig. 4.

The angular distribution of the observables described above were fit by expansions in terms of the appropriate Legendre and associated Legendre polynomials. The results are listed in Table I. As expected from charge symmetry, these results are similar to those from the ^{3}He$(\vec{d},\gamma)^5$Li reaction. Fits with $k > 2$ were not statistically justified, indicating no significant contributions by $E2$ radiation. The $k = 1$ coefficients suggest that a small amount of $E1$-$M1$ interference is present.

The results of a simultaneous TME fit to the observables are given in Tables I and III and shown in Fig. 4. As indicated from the Legendre fits, it was necessary to introduce a small amount of $M1$ radiation in order to fit the fore-aft asymmetry of the data, most notable in the $A_{yy}(\theta)$ data. As with the ^{3}He$(\vec{d},\gamma)^5$Li data in the fusion resonance region, two statistically significant solutions with nearly identical χ^2_ν=2.6 have been found, one with dominant $s = \frac{3}{2}$ s-wave capture strength, the second with $s = \frac{1}{2}$ and $\frac{3}{2}$ s-wave strengths, which contribute nearly equally to the capture cross section.

D. CCRGM calculations

One of the problems encountered when modeling nuclear reactions is that of effectively manipulating the large number of degrees of freedom. The coupled-channels resonating group model (CCRGM), which was first proposed by Wheeler [39] accomplishes this by clustering nucleons into bound substructures which have no internal degrees of freedom. The total wave function is then described as a linear combination of cluster wave functions multiplied by their respective relative-motion wave functions [40]. These wave functions are totally antisymmetrized in order to adhere to the Pauli principle and are optimized according to the prescription of the variational principle. Thus, the calculations can be improved by expanding the model space to include more clusters or more sophisticated internal cluster wave functions.

In the current CCRGM calculation, ^{5}Li (or ^{5}He) is described by d+^{3}He and p+^{4}He (or d+^{3}H and n+^{4}He) cluster wave functions. The proton and neutron are described simply as point particles. The d, ^{3}H, and ^{3}He cluster wave functions have a more complicated radial expression of the form:

$$\Psi(r) = \Sigma C_i e^{-b_i r^2}, \tag{12}$$

with one or two terms in the sum for each cluster. The C_i and b_i coefficients for the present case were obtained using the Ritz variational principle [41] and therefore yield upper bounds on the binding energy of each cluster.

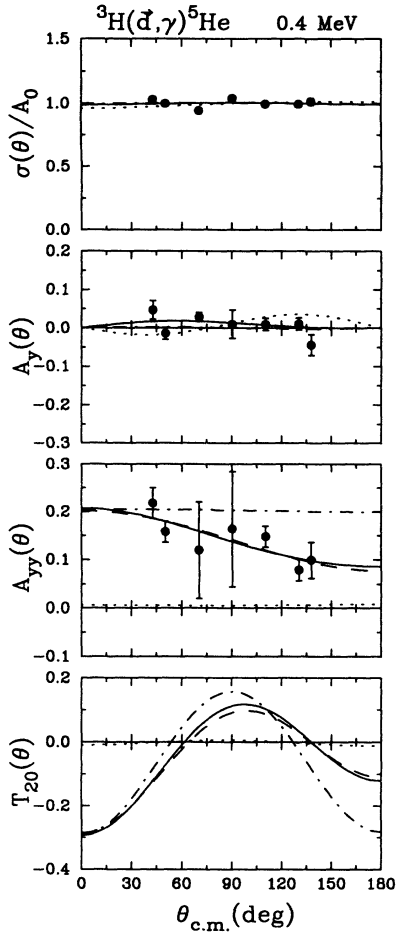

FIG. 4. Observables measured for the ^{3}H($\vec{d},\gamma$)^{5}He reaction at E_d(lab)=0.4 MeV where the beam was stopped in the target. The curves are the results of transition matrix element fits to the data. The solid and dashed curves represent solutions 1 and 2, respectively, of Table III. The dashed-dotted and dotted curves are from CCRGM calculations A (with the two-body tensor force) and D (no tensor force).

For the description of the ^{5}Li ground state, three cluster configurations have been used: $(p+^4\text{He})^{S=1/2}$, $(d+^3\text{He})^{S=1/2}$, and $(d+^3\text{He})^{S=3/2}$, where the cluster pairs are in a relative P state and their total angular momentum is $J=\frac{3}{2}$. Three cluster configurations have similarly been defined for ^{5}He where a neutron has replaced the proton and ^{3}H has replaced ^{3}He. The radial wave function for each cluster pair is then described by

$$|\alpha Lm\rangle = (\Psi_1\Psi_2)Y_{Lm}e^{-\gamma r^2}, \tag{13}$$

where α denotes the cluster configuration, $L=1$, and the Ψ_i represent the internal cluster wave functions obtained using Eq. (12). The coefficient γ in the exponential determines the distance between the two clusters. For a bound nucleus, γ can also be used as a free parameter in the variational calculation. However, the ^{5}Li and ^{5}He ground states are unbound in the $N+^4$He channel (where N is a proton or neutron) so that if the distance between the ^{4}He and N clusters is used as a free parameter in the variational calculation, the result is an infinite separation between them. It was therefore necessary to fix the distance between the clusters to values that reproduced the binding energy of ^{5}Li and ^{5}He reasonably well. The calculated binding energy of ^{5}Li is -20.75 MeV, which underestimates the experimental value of -26.33 MeV (determined from the peak of the ground-state resonance). For ^{5}He the calculated binding energy is -20.66 MeV, which underestimates the experimental value of -25.18 MeV. This variational calculation was carried out using the formalism of Ref. [42] with a phenomenological soft-core nucleon-nucleon potential [41].

The overlap integral of each cluster configuration with the total ground-state wave function is defined as

$$\text{Overlap integral} = \frac{\langle\alpha|A=5\rangle}{\sqrt{\langle\alpha|\alpha\rangle}\sqrt{\langle A=5|A=5\rangle}}, \tag{14}$$

where $|\alpha\rangle$ represents one of the three cluster-configuration wave functions and $|A=5\rangle$ represents the total ^{5}Li or ^{5}He ground-state wave function. According to the CCRGM calculations, the ^{5}Li and ^{5}He nuclei are almost entirely (>99.8%) in the $(\text{N}+^4\text{He})^{S=1/2}$ configuration, which is consistent with the shell-model description. Nonzero values for the $(d+^3\text{He})^{S=1/2}$ and $(d+^3\text{H})^{S=1/2}$ overlaps are due to the nonorthogonality of the two $S=\frac{1}{2}$ configurations in each calculation. Although the $(d+^3\text{He})^{S=3/2}$ and $(d+^3\text{H})^{S=3/2}$ overlaps increase if the tensor-force strength is increased, their contribution to the total wave function in any case is negligible ($\sim 10^{-4}$%). The scattering wave function is described by the same cluster configurations which were used to describe the ground states; however, all values of j^π that are allowed by the angular-momentum coupling algebra are included.

In order to determine the position of the $\frac{3}{2}^+$ resonances

TABLE III. Relative contributions of transition matrix elements to the cross section from a TME fit to the cross section and analyzing powers of the ^{3}H($\vec{d},\gamma$)^{5}He reaction in the fusion resonance region. The phase of the $^4s_{3/2}(E1)$ matrix element has been arbitrarily set to zero.

	^{3}H($\vec{d},\gamma$)^{5}He at E_d(lab)=0.4–0.0 MeV TME fits			
	Solution 1 χ^2_ν=2.61		Solution 2 χ^2_ν=2.58	
TME	Intensity	Phase	Intensity	Phase
$^2s_{1/2}(E1)$	0.03±0.03	147°±21°	0.44±0.16	67° ± 21°
$^4s_{3/2}(E1)$	0.88±0.05	0°	0.50±0.17	0°
$^2p(M1)$	0.05±0.05	55°±19°	0.04±0.03	−23° ± 21°
$^4p(M1)$	0.04±0.02	25°±12°	0.03±0.02	−158° ± 5°

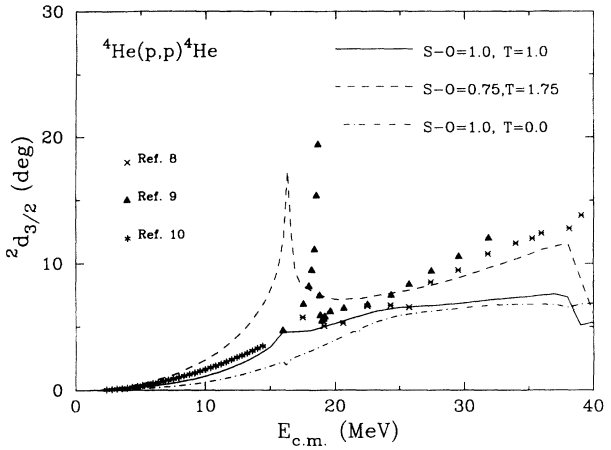

FIG. 5. The $^2d_{3/2}$ phase shift for the ^{4}He$(d,d)^4$He reaction. The data are taken from Refs. [8–10]. The curves represent CCRGM calculations with different tensor-force strengths. In the figure, S-O and T are factors which multiply the spin-orbit and tensor-force two-body strengths, respectively.

in the CCRGM model calculations, phase shifts were calculated for the ^{4}He$(p,p)^4$He and ^{4}He$(n,n)^4$He reactions. The calculated $^2d_{3/2}$ phase shift for the ^{4}He$(p,p)^4$He reaction is compared to the experimentally determined phase shifts [8–10] in Fig. 5. In this figure, T and S-O denote the fraction of the two-body tensor force and spin-orbit strength, respectively, used in the calculation. The fusion resonance is clearly evident although an increase in the tensor-force strength to $T = 1.75$ times the two-body strength is necessary for agreement with the size of the effect seen in the data. Even then the position of the resonance, which is determined primarily by the central force, is not correct.

In order to calculate the electromagnetic transitions, the scattering wave functions were calculated at the model-determined resonance position. The calculation of the electromagnetic transition matrix elements were then corrected for the discrepancy between the experimental and theoretical on-resonance γ-ray energies. Transition matrix elements for the ^{3}He$(\vec{d},\gamma)^5$Li and the ^{3}H$(\vec{d},\gamma)^5$He reactions were calculated at the $\frac{3}{2}^+$ fusion resonance (see Tables I and IV) for $E1$, $M1$, and $E2$ transitions using the two-body potential (calculation A for each reaction) and the phase-shift fitted potential (calculation B for each reaction). Additionally, $M2$ transitions were calculated for the ^{3}He$(\vec{d},\gamma)^5$Li reaction but were found to have negligible strength. Calculation A is shown in Figs. 3 and 4. Both of these calculations yielded nearly identical analyzing powers, which reproduce the measured analyzing powers of both reactions. Although these calculations were performed at the peak of the fusion resonance, energy averaging over the resonance, in accordance with the experimental conditions, does not change the theoretical results for the analyzing powers substantially since almost identical results were obtained at other energies in the averaging region. However, unlike the analyzing powers, the cross-section calculations overestimate the data dramatically (see Table I), even when energy averaging is considered. When compared to the measured on-resonance cross sections of Refs. [16,17], calculation A for the ^{3}He$(\vec{d},\gamma)^5$Li reaction still overestimates the cross section by a factor of 2 and 5, respectively. It is interesting to note that a factor of 2 reduction in the calculated cross section can be obtained by reducing the tensor-force strength to 0.75 times its two-body value (calculation C). This reduction does not lead to any appreciable discrepancies with the measured analyzing powers.

In calculations A, B, and C for the ^{3}He$(\vec{d},\gamma)^5$Li reaction, the $^4s_{3/2}(E1)$ transition matrix element dominates the capture cross section, contributing 98.5%, 99.8%, and 97.1% of the cross-section strength, respectively. Likewise, for the ^{3}H$(\vec{d},\gamma)^5$He reaction, this transition matrix element contributes 99.6% and 99.2% for calculations A and C. This effect is also responsible for the insensitivity of the analyzing powers to the different values of the tensor-force strength, resulting in analyzing powers that closely resemble the predictions from Eqs. (10) and (11) for the reaction proceeding only through $^4s_{3/2}(E1)$ capture. The mechanism responsible for this large amplitude works via the tensor force which couples the $(d{+}^3\mathrm{He})^{s=3/2}_{j=3/2}$ scattering channel to the $(p{+}^4\mathrm{He})^{s=1/2}_{j=3/2}$ scattering channel, allowing the transition

TABLE IV. Results of the coupled-channels resonating group model calculations in the fusion resonance region for calculation A using the two-body potential, and calculation D using the two-body potential with the tensor force turned off. Calculations B and C for each reaction are similar to calculation A. Transition matrix elements $^4d_{1/2}(E1)$, $^4d_{3/2}(E1)$, $^2p_{1/2}(M1)$, $^2p_{3/2}(M1)$, $^4p_{1/2}(M1)$, $^4p_{3/2}(M1)$, $^4p_{5/2}(M1)$, $^4p_{1/2}(E2)$, $^4p_{3/2}(E2)$, and $^4p_{5/2}(E2)$ were also calculated but are predicted to be essentially zero.

	CCRGM calculations							
	^{3}He$(\vec{d},\gamma)^5$Li				^{3}H$(\vec{d},\gamma)^5$He			
	A		D		A		D	
TME	Intensity	Phase	Intensity	Phase	Intensity	Phase	Intensity	Phase
$^2s_{1/2}(E1)$	0.013	96°	0.913	−84°	0.004	−85°	0.991	96°
$^4s_{3/2}(E1)$	0.985	70°	0.001	−98°	0.996	−128°	0.001	82°
$^2d_{3/2}(E1)$	0.000	−50°	0.001	133°	0.000	87°	0.000	−83°
$^2d_{5/2}(E1)$	0.000	−55°	0.006	126°	0.000	89°	0.000	−91°
$^4d_{5/2}(E1)$	0.000	−45°	0.000	−40°	0.000	103°	0.006	106°
$^2p_{1/2}(E2)$	0.000	123°	0.013	−58°	0.000	102°	0.000	−77°
$^2p_{3/2}(E2)$	0.001	−89°	0.064	93°	0.000	−114°	0.001	66°

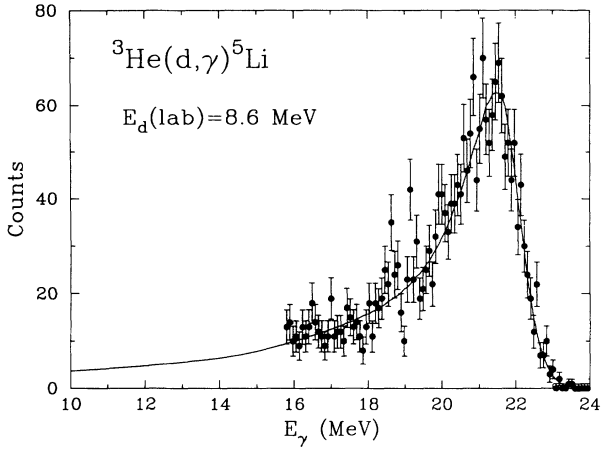

FIG. 6. A typical γ-ray spectrum from the ^{3}He$(d,\gamma)^5$Li reaction at E_d(lab)=8.6 MeV. The curve is from a convolution fit to the data as described in the text. The spectrum is cut off below 16 MeV.

to the $S=\frac{1}{2}$ ground state to proceed via the dominant spin-independent term of the $E1$ operator. To further examine the sensitivity of the calculation to the tensor force, a fourth calculation (calculation D) was performed with the tensor force turned off (see Figs. 3–5). In this case the tensor analyzing powers nearly vanish, the vector analyzing power becomes quite large, and the calculated cross section underestimates the measured cross sections by a factor of 16. These results differ from those of calculations A, B, and C due to the dramatic reduction in the strength of the $^4s_{3/2}(E1)$ transition matrix element which now contributes less than 1% of the calculated cross-section strength.

TABLE VI. Transition matrix element relative intensities from a TME fit to the cross section and analyzing powers of the ^{3}He$(\vec{d},\gamma)^5$Li reaction at E_d=8.6 MeV. Only one statistically significant solution (with $\chi^2_\nu=0.7$) has been found. The phase of the $^4s_{3/2}$ ($E1$) matrix element has been arbitrarily set to zero.

TME	Intensity	Phase
$^2s_{1/2}(E1)$	0.15±0.02	53° ± 5°
$^4s_{3/2}(E1)$	0.65±0.03	0°
$^2p(E2)$	0.00±0.00	133° ± 6°
$^4p(E2)$	0.00±0.00	179° ± 13°
$^2d(E1)$	0.18±0.02	199° ± 3°
$^4d(E1)$	0.02±0.01	72° ± 4°

IV. E_d=8.6 MeV

A. The ^{3}He$(\vec{d},\gamma)^5$Li reaction

Three reaction observables were measured at this energy [$\sigma(\theta)$, $A_y(\theta)$, and $A_{yy}(\theta)$]. A typical γ-ray spectrum is shown in Fig. 6. A γ-ray spectrum with no gas in the target chamber was also taken to determine the background due to the entrance and exit foils. No background was detected in the energy range of interest. The γ-ray spectra from the ^{3}He$(\vec{d},\gamma)^5$Li reaction were fit with a convolution of the NaI line-shape response function and a Breit-Wigner one-level approximation [38].

Legendre fits to the three measured observables [$\sigma(\theta)$,

TABLE V. Legendre polynomial coefficients for the ^{3}He$(\vec{d},\gamma)^5$Li reaction and the ^{3}H$(\vec{d},\gamma)^5$He reaction at E_d=8.6 MeV from a TME fit to the data and the CCRGM calculations. Calculation E uses the two-body potential. Calculation F uses the modified potential which has been adjusted to reproduce the ^{4}He$(p,p)^4$He phase shifts. Calculation G uses the two-body potential with no tensor force. A_0 is given in units of μb/sr. Coefficients from a direct fit of Legendre polynomials to the data are given in the footnote when they differ by more than one standard deviation from the TME-fit results.

	^{3}He$(\vec{d},\gamma)^5$Li				^{3}H$(\vec{d},\gamma)^5$He		
	TME fit	RGM E	RGM F	RGM G	TME fit	RGM E	RGM G
A_0	2.15 ±0.082	4.96	7.82	3.07	1.00 ±0.016	45.556	19.996
$\bar{a}_1$	−0.140 ±0.014	0.018	0.025	0.002	0.087 ±0.020[a]	−0.009	−0.008
$\bar{a}_2$	−0.205 ±0.024	−0.086	0.070	−0.189	−0.201 ±0.019	−0.077	−0.368
$\bar{a}_3$	−0.025 ±0.012	0.323	0.201	0.500			
$\bar{a}_4$	0.000 ±0.000[b]	0	0	0			
$\bar{b}_1$	−0.015 ±0.018	−0.107	−0.053	0.021	−0.009 ±0.009	0.002	0.005
$\bar{b}_2$	−0.023 ±0.009	0.122	0.127	−0.034	−0.076 ±0.006[a]	0.114	−0.014
$\bar{b}_3$	0.007 ±0.003	−0.012	−0.003	−0.025			
$\bar{b}_4$	0.000 ±0.000[b]	0	0	0			
$\bar{c}_0$	0.229 ±0.019	−0.004	−0.143	0.018	−0.049 ±0.010[a]	0.009	0.033
$\bar{c}_1$	−0.036 ±0.005	−0.036	−0.059	−0.004	−0.043 ±0.009	0.003	0.002
$\bar{c}_2$	−0.198 ±0.015	−0.273	−0.344	−0.006	−0.068 ±0.006[a]	−0.306	−0.012
$\bar{e}_2$	−0.111 ±0.006	−0.004	−0.024	−0.005	−0.023 ±0.002	0.002	−0.009

[a] $\bar{a}_1=0.062\pm0.013$, $\bar{b}_2=-0.053\pm0.014$, $\bar{c}_0=-0.035\pm0.009$, $\bar{c}_2=-0.025\pm0.031$.
[b] $\bar{a}_4=0.010\pm0.034$, $\bar{b}_4=-0.006\pm0.005$.

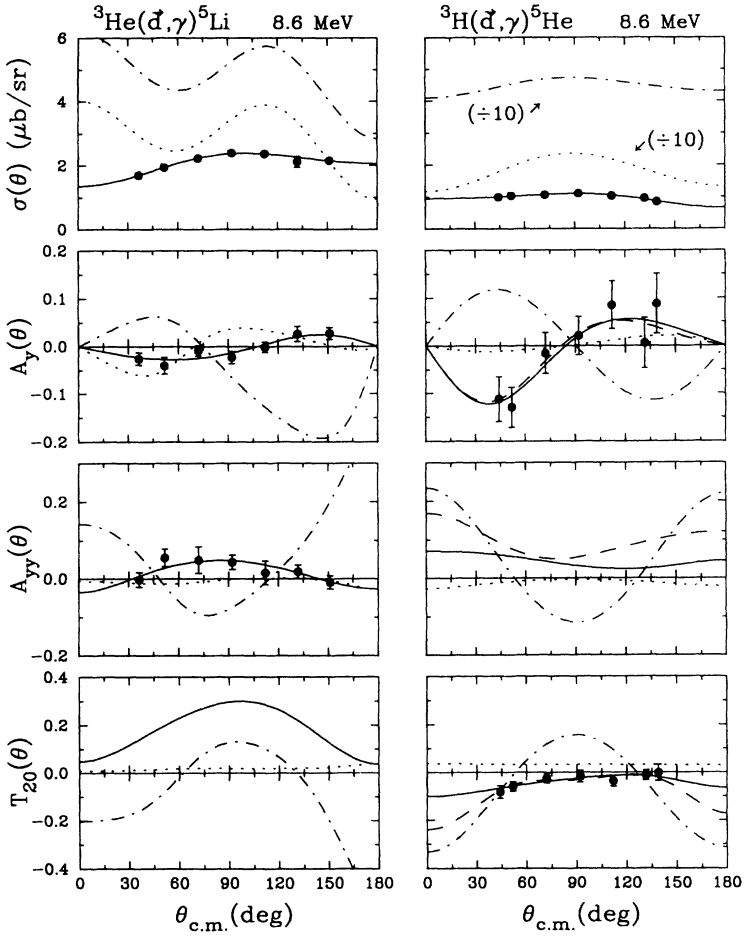

FIG. 7. Left side: Observables measured for the ^{3}He($\vec{d},\gamma$)^{5}Li reaction at E_d(lab)=8.6 MeV. The solid curve is the result of a transition matrix element fit to the data (see Table VI). The dashed-dotted and dotted curves are from CCRGM calculations E (with the two-body tensor force) and G (no tensor force). Right side: Observables measured for the ^{3}H($\vec{d},\gamma$)^{5}He reaction at E_d(lab)=8.6 MeV. The solid and dashed curves are from transition matrix element fits corresponding to solutions 1 and 2, respectively (see Table VII). The dashed-dotted and dotted curves are from CCRGM calculations E (with the two-body tensor force) and G (no tensor force). Note that the actual CCRGM cross sections are a factor of 10 higher than what is plotted.

$A_y(\theta)$, and $A_{yy}(\theta)$] have been performed. The results are given in Table V. The finite odd coefficients indicate $E1$-$M1$ and/or $E1$-$E2$ interference while the non-negligible $\bar{a}_3$ coefficient suggests some contributions from $E1$-$E2$ interference.

At E_d=8.6 MeV, only one TME solution (with χ^2_ν=0.7) was found from a fit to the cross section and analyzing powers $A_y(\theta)$ and $A_{yy}(\theta)$. The fit indicates that the capture cross-section strength is dominated by s-wave $E1$ capture with an admixture of ~20% d-wave $E1$ capture. The results of a simultaneous TME fit to all of the data are given in Table VI and shown in Fig. 7.

B. The ^{3}H($\vec{d},\gamma$)^{5}He reaction

For this reaction, background spectra were measured and subtracted from the spectra obtained with a tritiated foil using the technique described in Sec. II. A typical background-subtracted spectrum is shown in Fig. 8. The background-subtracted γ-ray spectra were fit with the measured line-shape response function of the NaI spectrometers. No convolution was used in the fitting. The cross section $\sigma(\theta)$, the vector analyzing power $A_y(\theta)$, and the tensor analyzing power $T_{20}(\theta)$ have been measured and are plotted in Fig. 7.

Adequate Legendre polynomial fits were obtained using polynomials of order $k \leq 2$. The results are given in Table V. TME fits to the data yield two solutions with nearly equal χ^2_ν=1.1. The results of these fits are given in Table VII and presented in Fig. 7. In both fits, about 20% of the cross-section strength is due to the $^4s_{3/2}(E1)$ matrix element. However, one fit indicates more than 40% of the cross section is contributed by d-wave capture while the other fit suggests only a ~15% contribution, where most of the remaining strength is produced by the $^2s_{1/2}(E1)$ and p-wave ($E2$) transitions. Interestingly, al-

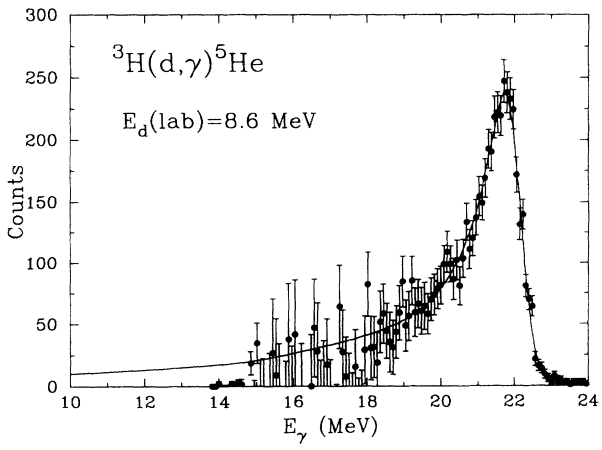

FIG. 8. A typical γ-ray spectrum for the ^{3}H(d,γ)^{5}He reaction at E_d(lab)=8.6 MeV. The curve is from a fit to the data.

TABLE VII. Transition matrix element relative intensities from a TME fit to the cross section and analyzing powers of the $^3\mathrm{H}(\vec{d},\gamma)^5\mathrm{He}$ reaction at E_d=8.6 MeV. Two statistically significant solution (with χ^2_ν = 1.1) have been found. The phase of the $^4s_{3/2}(E1)$ matrix element has been arbitrarily set to zero.

	$^3\mathrm{H}(\vec{d},\gamma)^5\mathrm{He}$ at E_d(lab)=8.6 MeV TME fits			
	Solution 1 χ^2=11		Solution 2 χ^2=11	
TME	Intensity	Phase	Intensity	Phase
$^2s_{1/2}(E1)$	0.25 ±0.03	109 ±15	0.43±0.10	109 ±8
$^4s_{3/2}(E1)$	0.20 ±0.04	0	0.23±0.05	0
$^2p(E2)$	0.003 ±0.002	134 ±38	0.10±0.02	188 ±7
$^4p(E2)$	0.02 ±0.01	75 ±14	0.10±0.03	91 ±7
$^2d(E1)$	0.43 ±0.05	356 ±11	0.10±0.02	46 ±12
$^4d(E1)$	0.10 ±0.01	155 ±24	0.05±0.01	220 ±12

though two solutions were found, neither one closely resembles the solution found for the $^3\mathrm{He}(\vec{d},\gamma)^5\mathrm{Li}$ data although a comparable solution was explicitly sought.

C. CCRGM calculations

Transition matrix elements have been calculated for the $^3\mathrm{He}(\vec{d},\gamma)^5\mathrm{Li}$ and the $^3\mathrm{H}(\vec{d},\gamma)^5\mathrm{He}$ reactions at E_d(lab)=8.6 MeV using the two-body potential (calculation E), the phase-shift adjusted potential (calculation F), and the two-body potential where the tensor-force strength has been turned off (calculation G). All of the parameters of the calculations are the same as those used for the calculations in the fusion resonance region. The results of these calculations are listed in Tables V and VIII and are plotted in Fig. 7. At this energy, qualitative agreement with the measured cross sections and analyzing powers was improved by turning off the tensor force (calculation G). However, a comparison of transition matrix elements reveals that although the calculated observables reproduce the data better, the relative intensities of the transition matrix elements do not agree with those extracted from a TME fit to the data. In fact, a nonzero tensor force is necessary to get even a rough agreement between the data and theory for the relative strengths of the TME's. For the $^3\mathrm{H}(\vec{d},\gamma)^5\mathrm{He}$ reaction, calculation E (with 43% s-wave $E1$ capture and 57% d-wave $E1$ capture) suggests that the TME Solution 1 (with 45% s-wave $E1$ capture and 53% d-wave $E1$ capture) is the physical one, although the spin dependence of the two s-wave TME's is not reproduced. As with the CCRGM calculation at the peak of the fusion resonance, the $^4s_{3/2}(E1)$ transition matrix element contributes strongly to the capture cross section via the coupling of the $[d+^3\mathrm{He}\ (\text{or}\ ^3\mathrm{H})]^{s=3/2}_{j=3/2}$ scattering channel to the $(N+^4\mathrm{He})^{s=1/2}_{j=3/2}$ scattering channel by the tensor force. For both reactions, calculation E predicts that the $^4d_{3/2}(E1)$ TME contributes 4% and 10%, respectively, to the cross section via this same tensor-force coupling mechanism, while the $^2d_{5/2}(E1)$ TME contributes 40% and 39%, respectively, to the cross section by coupling directly to the $N+^4$He channel. Small to zero amounts of $M1$ or $E2$ radiation are predicted.

V. CONCLUSION

The experimental results reported in this paper comprise the first study of the $^3\mathrm{He}(\vec{d},\gamma)^5\mathrm{Li}$ and the

TABLE VIII. Results of the coupled-channels resonating group model calculations at E_d(lab)=8.6 MeV for calculation E using the two-body potential, and calculation G using the two-body potential with the tensor force turned off. Calculation F for each reaction is similar to calculation E. Transition matrix elements $^2p_{1/2}(M1)$, $^2p_{3/2}(M1)$, $^4p_{1/2}(M1)$, $^4p_{3/2}(M1)$, $^4p_{5/2}(M1)$, $^4p_{3/2}(E2)$, and $^4p_{5/2}(E2)$, were also calculated but are predicted to be essentially zero.

	CCRGM calculations							
	$^3\mathrm{He}(\vec{d},\gamma)^5\mathrm{Li}$				$^3\mathrm{H}(\vec{d},\gamma)^5\mathrm{He}$			
	E		G		E		G	
TME	Intensity	Phase	Intensity	Phase	Intensity	Phase	Intensity	Phase
$^2s_{1/2}(E1)$	0.019	142°	0.034	−38°	0.003	−33°	0.008	142°
$^4s_{3/2}(E1)$	0.308	6°	0.000	−66°	0.430	166°	0.000	114°
$^2d_{3/2}(E1)$	0.061	175°	0.101	−4°	0.037	−18°	0.088	161°
$^2d_{5/2}(E1)$	0.398	165°	0.647	−14°	0.388	−29°	0.896	151°
$^4d_{1/2}(E1)$	0.033	−23°	0.000	63°	0.032	141°	0.000	−126°
$^4d_{3/2}(E1)$	0.043	−85°	0.000	125°	0.095	71°	0.000	−75°
$^4d_{5/2}(E1)$	0.001	117°	0.002	111°	0.014	−72°	0.007	−86°
$^2p_{1/2}(E2)$	0.003	27°	0.009	−155°	0.000	2°	0.000	182°
$^2p_{3/2}(E2)$	0.127	157°	0.205	−23°	0.000	151°	0.001	−29°
$^4p_{1/2}(E2)$	0.004	57°	0.000	53°	0.000	37°	0.000	−5°

^{3}H($\vec{d},\gamma$)^{5}He reactions. Measurements were obtained at E_d(lab)=8.6 MeV as well as for deuteron energies which encompassed the fusion resonance regime.

The 8.6 MeV data appear to be better described by a coupled-channels resonating group model (CCRGM) calculation with the tensor force turned off. However, the strong s-wave $E1$ capture strength obtained in the transition matrix element analysis requires the tensor force to be present, although this calculation fails to describe our data.

In the case of the fusion resonance region, the CCRGM model gives a good description of the data if a tensor force having 0.75 times the two-body tensor-force strength is included. Although this calculation overpredicts our measured cross section by a factor of 2, it agrees with a previous measurement of Ref. [16]. Increasing the tensor-force strength increases the predicted cross section, but the analyzing powers stay in good agreement with the data. If the tensor force is turned off then the tensor analyzing powers go essentially to zero and the cross section is more than an order of magnitude too small. This result indicates that the tensor force is the driving force in the ^{3}He($\vec{d},\gamma$)^{5}Li and ^{3}H($\vec{d},\gamma$)^{5}He reactions at these low energies. Since the ^{3}He$(d,\gamma)^5$Li-to-^{3}He$(d,p)^4$He and ^{3}H$(d,\gamma)^5$He-to-^{3}H$(d,n)^4$He branching ratios are flat in the region of the fusion resonance, the present study also shows that the tensor force drives the energy-producing (d,n) and (d,p) reactions. Furthermore, the effects of the tensor force dramatically increase the feasibility of using the ^{3}He$(d,\gamma)^5$Li reaction as a diagnostic tool for deuterium-tritium reactors.

ACKNOWLEDGMENTS

The authors wish to thank Z. D. Huang, L. H. Kramer, J. L. Langenbrunner, R. M. Whitton, J. Z. Williams, and V. Wijekumar for their assistance in the collection of the data presented here. We also wish to thank H. M. Hofmann and M. Unkelbach for numerous enlightening discussions about the CCRGM calculations. These calculations would not have been possible without their generous assistance. This work was supported in part by the U.S. Department of Energy, Office of High Energy and Nuclear Physics, under Contract No. DEFG05-91-ER40619.

[1] F. E. Cecil, D. M. Cole, F. J. Wilkinson III, and S. S. Medley, Nucl. Instrum. Methods **B10/11**, 411 (1985).
[2] T. W. Bonner, J. P. Conner, and A. B. Lillie, Phys. Rev. **88**, 473 (1952).
[3] G. Freier and H. Holmgren, Phys. Rev. **93**, 825 (1954).
[4] J. L. Yarnell, R. H. Lovberg, and W. R. Stratton, Phys. Rev. **90**, 292 (1953).
[5] G. G. Ohlsen *et al.*, in *Polarization Phenomena in Nuclear Reactions*, edited by H. H. Barschall and W. Haeberli (University of Wisconsin Press, Madison, Wisconsin, 1971), pp. 305 and 842.
[6] H. A. Grunder, R. Gleyvod, J. Lietz, G. Morgan, H. Rudin, F. Seiler, and A. Stricker, Helv. Phys. Acta **44**, 662 (1971).
[7] J. P. Conner, T. W. Bonner, and J. R. Smith, Phys. Rev. **88**, 468 (1952).
[8] A. Houdayer, N. E. Davidson, S. A. Elbakr, A. M. Sourkes, W. T. H. Van Oers, and A. D. Bacher, Phys. Rev. C **18**, 1985 (1978).
[9] G. R. Plattner, A. D. Bacher, and H. E. Conzett, Phys. Rev. C **5**, 1158 (1972).
[10] P. Schwandt, T. B. Clegg, and W. Haeberli, Nucl. Phys. **A163**, 432 (1971).
[11] A. G. M. Van Hees and P. W. M. Glaudemans, Nucl. Phys. **A396**, 105c (1983).
[12] J. Burger, H. M. Hofmann, H. Kellermann, and T. Mertelmeier, in *Proceedings of the International Conference on Nuclear Physics*, edited by P. Blasi and R. A. Ricci (Tipografia Compositori, Bologna, 1983), Vol. 1, p. B9.
[13] H. M. Hofmann (private communication).
[14] G. Blüge and K. Langanke, Few Body Systems **11**, 137 (1991).
[15] G. Blüge and K. Langanke, Phys. Rev. C **41**, 1191 (1990).
[16] J. M. Blair, N. M. Hintz, and D. M. Van Patter, Phys. Rev. **96**, 1023 (1954).
[17] W. Buss, W. Del Bianco, H. Wäffler, and B. Ziegler, Nucl. Phys. **A112**, 47 (1968).
[18] L. Kraus, M. Suffert, and D. Magnac-Valette, Nucl. Phys. **A109**, 593 (1968).
[19] W. Buss, H. Waffler, and B. Ziegler, Phys. Lett. **4**, 198 (1963).
[20] A. Kosiara and H. B. Willard, Phys. Lett. **32B**, 99 (1970).
[21] V. M. Bezotsnyi, V. A. Zhmaylo, L. M. Surov, and M. S. Shvetsoy, Yad. Fiz. **10**, 225 (1969) [Sov. J. Nucl. Phys. **10**, 127 (1970)].
[22] F. E. Cecil, D. M. Cole, F. J. Wilkinson III, and S. S. Medley, Nucl. Instrum. Methods **B10/11**, 411 (1985).
[23] G. L. Morgan, P. W. Lisowski, S. A. Wender, R. E. Brown, N. Jarmie, J. F. Wilkerson, and D. M. Drake, Phys. Rev. C **33**, 1224 (1986).
[24] T. A. Tombrello, R. J. Spiger, and A. D. Bacher, Phys. Rev. **154**, 935 (1967).
[25] H. Schröder and W. Mausberg, Z. Phys. **235**, 234 (1970).
[26] W. Del Bianco, F. Lemire, F. J. A. Lévesque, and J. M. Poutissou, Can. J. Phys. **46**, 1585 (1968).
[27] H. T. King, Nucl. Phys. **A178**, 337 (1972).
[28] F. Ajzenberg-Selove, Nucl. Phys. **A490**, 1 (1988).
[29] J. C. Riley, H. R. Weller, and D. R. Tilley, Phys. Rev. C **40**, 1517 (1989).
[30] M. J. Balbes, G. Feldman, H. R. Weller, and D. R. Tilley, Phys. Rev. C **45**, R487 (1992).
[31] T. B. Clegg, G. A. Bissinger, and T. A. Trainor, Nucl. Instrum. Methods **120**, 445 (1974).
[32] T. B. Clegg, H. J. Karwowski, S. K. Lemieux, R. W. Sayer, E. R. Crosson, and W. M. Hooke (unpublished); D. C. Dinge, T. B. Clegg, E. R. Crosson, and H. W. Lewis (unpublished); T. B. Clegg, W. M. Hooke, E. R. Crosson, A. W. Lovette, H. Middleton, H. G. Pfutzner, and K. A. Sweeton (unpublished).
[33] K. Stephenson and W. Haeberli, Nucl. Instrum. Methods

169, 483 (1980).
[34] H. R. Weller and N. R. Roberson, IEEE Trans. Nucl. Sci. **NS-28**, 1268 (1981).
[35] S. E. King, N. R. Roberson, H. R. Weller, and D. R. Tilley, Phys. Rev. C **30**, 21 (1984).
[36] J. L. Langenbrunner, H. R. Weller, and D. R. Tilley, Phys. Rev. C **42**, 1214 (1990).
[37] R. G. Seyler and H. R. Weller, Phys. Rev. C **20**, 453 (1979).
[38] M. J. Balbes, G. Feldman, L. H. Kramer, H. R. Weller, and D. R. Tilley, Phys. Rev. C **43**, 343 (1991).
[39] J. A. Wheeler, Phys. Rev. **52**, 1083 (1937).
[40] H. M. Hofmann, *Resonating Group Calculations in Light Nuclear Systems*, Vol. 273 in *Lecture Notes in Physics* (Springer-Verlag, Berlin, 1986).
[41] T. Mertelmeier and H. M. Hofmann, Nucl. Phys. **A459**, 387 (1986).
[42] H. Eikemeier and H. H. Hackenbroich, Nucl. Phys. **A169**, 407 (1971).